

# Freeform surface topology prediction for prescribed illumination via semi-supervised learning

Jeroen Cerpentier<sup>1</sup> and Youri Meuret<sup>1,\*</sup>

<sup>1</sup>KU Leuven, Department of Electrical Engineering (ESAT), Light & Lighting Laboratory, B-9000 Gent, Belgium

\*Corresponding author: youri.meuret@kuleuven.be

## Abstract

Fast, effective design of freeform illumination components with extended light sources remains an open challenge, despite significant advances in the field. Machine learning techniques already proved to be extremely valuable in solving complex inverse problems in optics and photonics, but their application to freeform optical design is so far limited to imaging optics. This paper presents a rapid, standalone framework for the prediction of freeform surface topologies that generate a prescribed irradiance distribution, from an extended light source. The framework employs a 2D convolutional neural network to model the relationship between the prescribed target irradiance and required freeform topology. This network is trained on the loss between the obtained irradiance and input irradiance, using a second network that replaces Monte-Carlo ray-tracing from source to target. This semi-supervised learning approach proves to be superior compared to a supervised learning approach using ground truth freeform topology/irradiance pairs, a fact that is most likely connected to the observation that multiple freeform topologies can yield similar irradiance patterns. The resulting network is able to rapidly predict smooth freeform topologies that generate arbitrary, complex irradiance patterns.

## Introduction

Optical systems to control the propagation of light play a major role in science and technology, and their importance will not diminish in the near future [1, 2, 3]. For decades, optical engineers have relied on systems with

multiple (a)spherical surfaces, which have rotational symmetry [4, 5]. Recent advances in manufacturing technology however, allow the fabrication of freeform optical surfaces with completely arbitrary shape, thereby offering much greater flexibility for controlling the propagation of light [6, 7]. Freeform optics are widely used in imaging systems to guide the light of points in object space effectively to corresponding points in image space [8, 9, 10, 11]. Also in the field of illumination design, freeform components are extensively used to map the emitted light distribution from a source into a desired target pattern, while maintaining the luminous flux [12, 13]. The demand for such freeform illumination systems is rapidly growing, due to their application in fast-evolving fields such as optical lithography, automotive headlights and laser beam shaping [14, 15].

Illumination optics are determined by the light source under consideration and the targeted light pattern. Their design typically comes down to calculating one or more optical surfaces that manipulate the incoming rays, in order to produce a certain prescribed intensity or irradiance distribution. Freeform illumination design methods can be separated in two categories: zero-étendue algorithms and algorithms for extended light sources [14]. Zero-étendue methods are based on the assumption that the source is ideal, e.g. a point source or a collimated laser beam. Freeform design for zero-étendue sources has matured significantly, and various accurate calculation methods exist, such as the ray-mapping and Monge-Ampère methods [16, 17, 18, 19]. Unfortunately, the étendue of real light sources can seldom be neglected in practice. When applying zero-étendue algorithms for such extended light sources, the resulting pattern becomes blurry, and more dedicated design procedures are needed [20, 21].

As opposed to zero-étendue algorithms, the search for fast and effective freeform algorithms with extended light sources is still ongoing [14, 22]. Benitez et al. have expanded the simultaneous multiple surfaces (SMS) design method from 2D to 3D [23]. Alternatively, wavefront tailoring and deconvolution-based algorithms have been proposed [22, 24, 25]. Although these methods function well under certain specific conditions, e.g. single-chip LED emitters, they remain unsuitable for arbitrary extended light sources. Alternatively, a solution can be obtained through straight-forward optimization of the parameterized freeform surface(s), based on a defined merit function, e.g. the difference between the obtained irradiance and the target distribution [26, 27]. Similarly, feedback-based methods have been introduced, iteratively updating the solution with a continuous feedback mechanism [14, 28, 29]. Finally, the usage of automatic differentiation has been proposed to obtain derivative information of optical surface parame-

ters. This information allows for more rapid and effective optimization of freeform systems [30, 31], but research on applying such methods for illumination design is still in an early phase [32, 33, 34]. All these iterative methods have the potential to result in appropriate illumination optics for extended light sources. However, they are typically very computationally intensive and require a significant amount of convergence time.

To reduce the time and complexity of optical design, researchers have recently started to use machine learning techniques. Applying deep learning to solve inverse problems in photonics and optics has only recently arisen, but the potential is undisputable [35, 36, 37]. It may arguably become one of the main catalysts in designing complex optical configurations in the near future [38]. In the field of computational holography for example, mature machine learning methods are already state-of-the-art [39, 40].

Deep learning architectures for freeform design have also been presented in past research, but so far mainly within the domain of imaging optics, in order to find starting points close to a final solution [31, 41, 42, 43]. Within illumination design, only one fully trained network has been demonstrated and the approach was restricted to creating very basic shapes [44]. The authors of this work underlined the need for more advanced procedures. One of the main challenges to realize a fully trained network for freeform illumination design via supervised or unsupervised learning is the lack of a fast forward operator to link the input and output parameters. Monte-Carlo (MC) ray-tracing is typically used to evaluate the performance of freeform optics for a given (extended) light source. Given the complex shape that freeform surfaces can adopt, thousands to even millions of rays are needed to model the resulting intensity or irradiance pattern with limited statistical noise.

Aside from the considered light source and targeted light distribution, there is another aspect that is of practical importance in the design of freeform components for illumination purposes: the resulting freeform shape. Most freeform design methods result in convex or concave optical components (Fig. 1a). Such components may lead to visual discomfort glare when combined with high-brightness light sources [45]. A possible approach to address this important issue in lighting, is working with freeform lens arrays [46]. Unfortunately, such freeform lens arrays have strong C2 discontinuities in between the individual sub-lenses. These discontinuous complicate manufacturing and lead to unwanted straylight [47]. Such problems could be avoided with smooth freeform surfaces that combine multiple convex, concave and saddle shaped regions, for which we introduce the term *freeform topologies* (Fig. 1c). An additional advantage of such freeform lens topolo-

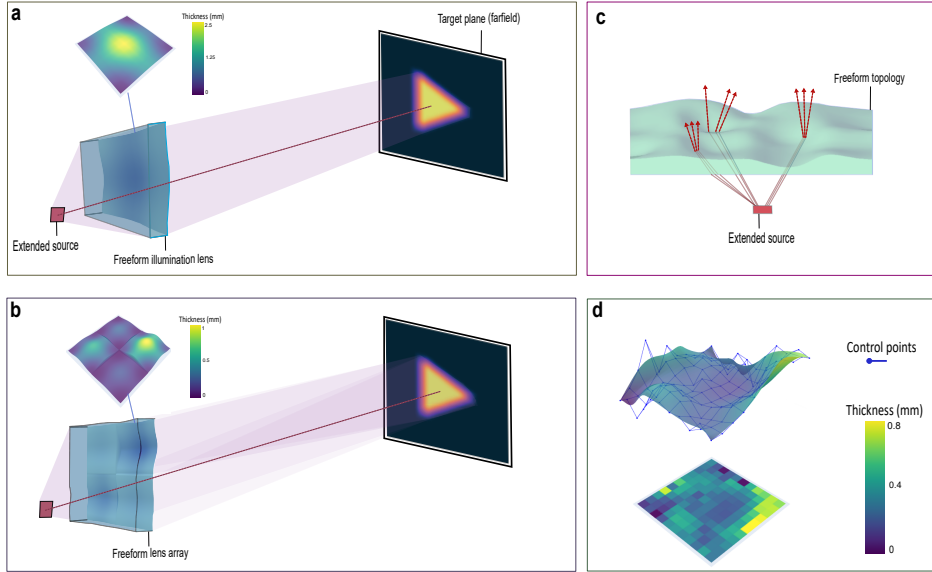


Figure 1: **(a)** Convex freeform illumination lens that generates a prescribed (far-field) target pattern from an extended light source. **(b)** The light patterns generated by each of the four individual sub-lenses of a discontinuous lens array result in the prescribed target pattern. **(c)** A smooth, continuous freeform surface *topology* that consists of multiple convex, concave and saddle-shaped regions avoids strong C2 discontinuities and results in a much thinner component. **(d)** A freeform surface topology can be described as a NURBS surface that is controlled via a matrix of control points.

gies in comparison with a single convex or concave freeform lens, is the limited component thickness. Even though this feature can also be achieved with freeform Fresnel lenses, these also exhibit discontinuous jumps [48]. Unfortunately, direct design methods for smooth, continuous freeform topologies are nonexistent at this moment.

This paper presents a deep learning framework for solving the inverse problem of finding a freeform lens surface topology in order to obtain a prescribed irradiance distribution with an extended light source. The framework integrates supervised learning for modeling the ray-tracing on one hand, and semi-supervised learning for freeform surface prediction on the other hand. This double approach alleviates the computational burden to train the freeform surface prediction fully via Monte-Carlo ray-tracing. We demonstrate that rapid convergence can be obtained by considering the deviation of the irradiance resulting from a predicted freeform surface with

the target irradiance as a loss function during training. This approach is radically different from the more intuitive method of considering the mean average error of the predicted freeform surface shape compared to the ground truth, which proves to have inferior convergence. This behavior is directly linked to the observation that two or more completely distinct freeform topologies can result in visually identical illumination patterns. The deep learning framework rapidly provides a suitable freeform design as is illustrated for various target patterns. As such, we demonstrate that deep learning does not only serve as a tool to enhance typical optimization procedures, but that it can be used as a rapid, standalone method in freeform lens design.

## Results

### Problem statement

Consider a freeform lens consisting of a planar entrance surface, orthogonal to the optical axis ( $z$ -axis) and a freeform exit surface. The freeform surface can be represented as a non-uniform rational basis spline (NURBS) surface with  $a \times b$  equidistant control points (Fig. 1d). When the  $x$ - and  $y$ -coordinates of these control points are predefined, only the  $z$ -coordinate is a free parameter that samples the local height of the freeform lens. With this parameterization, the freeform lens is fully characterized by an  $a \times b$  matrix ( $\mathcal{F}$ ). By restricting all  $z$ -coordinates to a certain interval  $[0, t]$ , the thickness of the freeform lens can be limited.

Light rays can be propagated from the source through the optical surfaces towards a detector surface. By binning the radiant flux of multiple light rays on this detector, in an  $m \times n$  spatial receiver grid, the irradiance distribution on the detector ( $\mathcal{I}$ ) can be sampled. A ray-tracing algorithm thus allows to construct the mapping

$$\{\mathcal{F} \in [0, t]^{a \times b}\} \rightarrow \{\mathcal{I} \in \mathbb{R}_+^{m \times n}\}. \quad (1)$$

The problem that is tackled in this work is modeling the inverse relation

$$\{\mathcal{I} \in \mathbb{R}_+^{m \times n}\} \rightarrow \{\mathcal{F} \in [0, t]^{a \times b}\} \quad (2)$$

i.e. for any random irradiance distribution  $\mathcal{I}$  on the target plane, predict the  $\mathcal{F}$  that results in  $\mathcal{I}$  via ray-tracing.

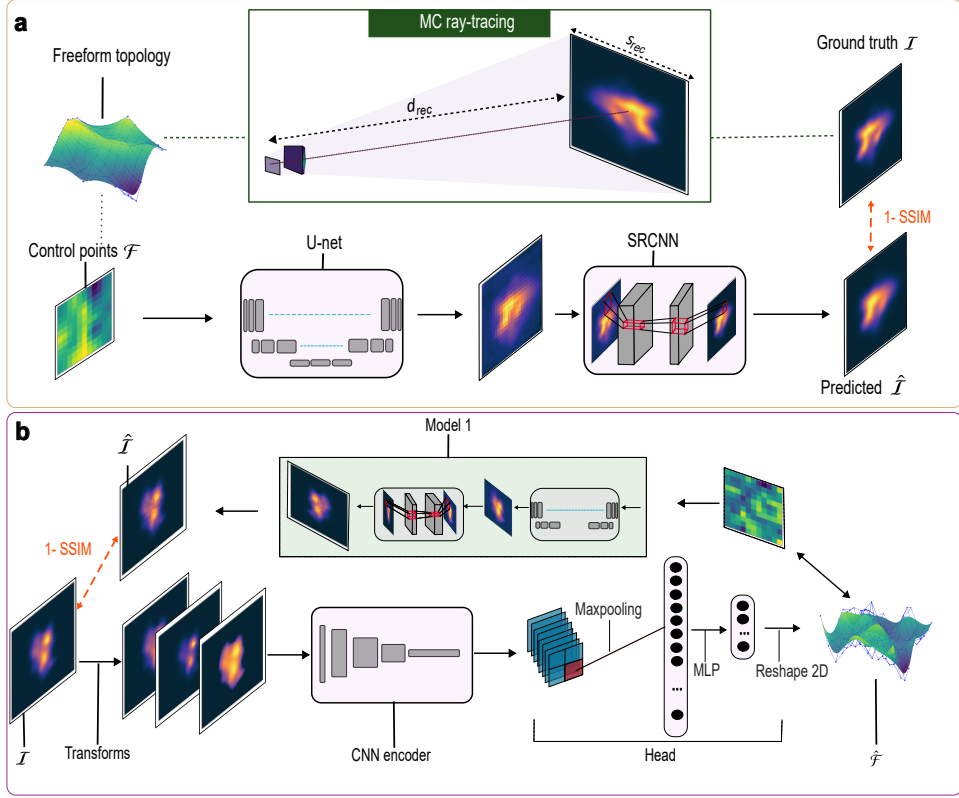


Figure 2: **(a)** Illustration of the U-net-SRCNN model for predicting the obtained irradiance on the target plane for a certain freeform surface. The model is trained by considering pairs of freeform topologies and the corresponding simulated far-field irradiance distributions, via MC ray-tracing. Training loss is evaluated using the SSIM loss between the MC-simulated ground truth  $\mathcal{I}$  and the U-net-SRCNN predicted  $\hat{\mathcal{I}}$ . **(b)** Illustration of the model to predict a freeform grid  $\hat{\mathcal{F}}$  from an input irradiance  $\mathcal{I}$ . Training is achieved by considering the SSIM loss between the input irradiance  $\mathcal{I}$  and  $\hat{\mathcal{I}}$ , which is the predicted irradiance of  $\hat{\mathcal{F}}$  by the first model.

## Framework structure

Our deep learning framework consists of two different architectures (Fig. 2a, 2b). The first deep learning architecture is a U-net that models the irradiance distribution on the receiver as a results of propagating light rays through the optical system. This architecture implements the mapping relation in Eq. (1) which is typically obtained with MC ray-tracing. U-nets are commonly used segmentation structures and are ideal for modeling 2D-to-2D

mappings. They are widely used in medical imaging and for image deconvolution [49, 50]. However, when tracing rays through arbitrary freeform surfaces, the resulting irradiance distribution often contains highly detailed features. U-nets generally predict images with relative low resolution, causing these high resolution features to vanish during prediction. To attain more detailed irradiance prediction, a super resolution CNN (SRCNN) is appended [51]. The full model, visualized in Fig. 2a, is trained on structural similarity index measure (SSIM) loss in a supervised manner [52]. The training data is generated using MC ray-tracing in a predefined setting. Moreover, significant data augmentation is performed by considering the inverse rotational symmetry of  $\mathcal{F}$  and  $\mathcal{I}$ .

The second network architecture is designed to model the mapping relation of Equation 2 and is schematically it shown in Fig. 2b, together with the considered learning strategy. This architecture consists of a typical CNN encoder network, containing a 2D max-pooling head and multi-layer perceptron regressor (MLP), thus predicting the surface parameters  $\hat{\mathcal{F}}$  for an input irradiance  $\mathcal{I}$  [53]. To ensure the prediction of a freeform surface topology that yields an irradiance distribution resembling the input irradiance, it is required to capture both the local and global characteristics of the input irradiance distributions  $\mathcal{I}$  in the training phase. This is achieved by feeding also the exponential and logarithmic transform of  $\mathcal{I}$  to the network, as a 3-channel input. The logarithmic transform allows the model to learn the global context of the input irradiance, whereas the exponential accentuates local irradiance peaks. The pre-trained U-net-SRCNN model is used in the training phase of this second network for two different tasks. First of all, it is used to produce a large set of input irradiance distributions for the learning phase of the second model, without needing to run a huge amount of MC ray-tracing simulations. The advantage of this approach compared to using completely arbitrary irradiance distributions, is that these distributions are a result of the considered freeform topology parameterization, and can thus in principle be obtained with the considered freeform lens. Secondly, the pre-trained ray-tracing model is used during the actual training phase to produce a pseudo-labeled irradiance  $\hat{\mathcal{I}}$  for any predicted  $\hat{\mathcal{F}}$  [54]. The assumption is that these generated pseudo-labels serve as legitimate irradiance distributions, accurately reflecting the MC ray-traced results. Their goal is to compare them with the input irradiance distributions during the training phase of model 2. So with  $m_1$  and  $m_2$  representing model 1 and model 2 respectively, the trainable loss  $\mathcal{L}$  is evaluated as:

$$\mathcal{L}\{\mathcal{I}, m_2(\mathcal{I})\} = 1 - \text{SSIM}\{\mathcal{I}, m_1[m_2(\mathcal{I})]\} = 1 - \text{SSIM}\{\mathcal{I}, m_1(\hat{\mathcal{F}})\}, \quad (3)$$

with  $m_1(\hat{\mathcal{F}})$  the generated pseudo-labeled irradiance to be compared with the ground truth  $\mathcal{I}$ . By including the (frozen) ray-tracing model in the training phase of the freeform prediction architecture, the emphasis of model 2 is on replicating the ground truth irradiance distribution, as opposed to replicating the ground truth freeform surface, which is not considered in the training of the second model.

This approach is somehow related to the unsupervised learning strategy that was adopted in computational holography, in favor of supervised learning using an extensive set of random phase masks paired with their simulated amplitude pattern [40]. A main difference is that computational holography can rely on an analytic forward/backward operator for the complex field at the image plane. For the considered case, the role of this analytic operator is taken over by the pre-trained U-net-SRCNN model.

## Prediction results

**Optical simulation setting** The framework is applied in a specific optical setting, to illustrate its usage and performance. An extended, planar light source of  $3 \times 3$  mm square is illuminating a freeform lens of  $10 \times 10$  mm square at a distance of 40 mm, with a planar entrance surface and freeform exit surface. The refractive index of the lens is 1.5, and a maximum lens thickness of  $t = 0.8$  mm is considered. The freeform lens redirects the incident light towards a square receiver plane at a distance of  $d_{rec} = 500$  mm and side length  $s_{rec} = 1000$  mm, i.e. in the far-field of the lens (see Fig. 2a). This configuration corresponds to the case were a compact LED illuminates a shallow freeform lens, and is e.g. representative for the illumination of a phase-only spatial light modulator that is implemented as a programmable freeform optic, by an extended light source [55]. The freeform surface is characterized by a matrix of  $11 \times 11$  equidistant control points of the corresponding NURBS surface [34]. In order to produce irradiance patterns that cover the entire target plane, freeform surface topologies with multiple hills and valleys are necessary. This is a direct consequence of the shallow lens thickness and the fact that large surface slopes are needed to realize the required deflection angles. This is only possible by combining multiple positive and negative surface slopes.

The dataset for supervised learning of the U-net is generated in the commercial software LightTools [56], which allows MC ray-tracing through

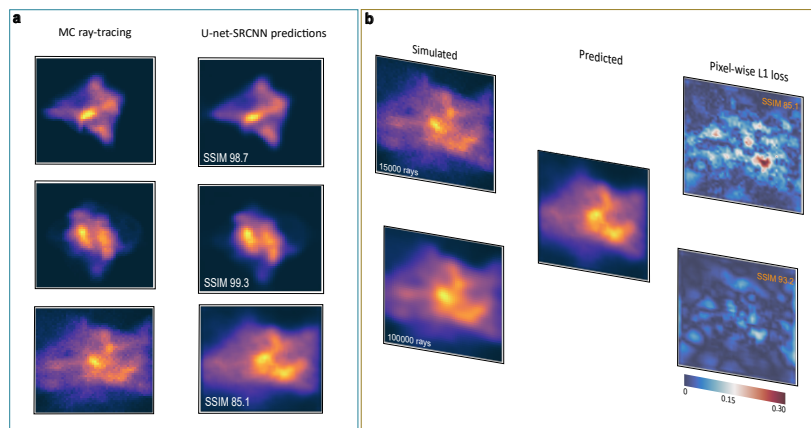


Figure 3: **(a)** MC-ray-tracing simulated irradiance versus predicted irradiance by the U-net-SRCNN model. The bottom image represents a low SSIM outlier in the validation set. **(b)** Pixel-wise error for the predicted irradiance compared to the ray-traced irradiance for a different number of MC-sampled rays. This illustrates that the model removes noise from the trained data.

freeform (NURBS) lens surfaces. To start, 25000 random freeform topologies are generated by selecting an arbitrary z-coordinate within the chosen interval for each lens surface control point. The corresponding irradiance distribution  $\mathcal{I}$  for each freeform topology  $\mathcal{F}$  is then calculated by tracing 15000 rays from the light source towards the receiver plane. Training is executed on the resulting  $\{\mathcal{F}, \mathcal{I}\}$  pairs, using a 90-10 train-validation split.

**Irradiance prediction** Fig. 3a shows quantitative and visual results for the U-net-SRCNN model. The predicted irradiance distribution by the model is compared with the corresponding Monte-Carlo ray-tracing result for three different cases, together with the SSIM loss. The bottom figure shows an outlier in terms of SSIM, compared to the average SSIM of the complete validation set, which is 98.3%. The average 1.7% error is mainly due to the simulation noise in the considered ray-tracing simulations. This noise is more significant for samples where the irradiance is spread out over the entire receiver plane. A more extensive simulated ray-set would be required to suppress these noise effects, but this turned out to be unnecessary. Indeed, in Figure 3b, the validation irradiance for the SSIM outlier of Figure 3a, simulated with 15000 rays, is compared with the MC simulated irradiance for the same freeform lens but with a rayset of 1 million rays. Taking the absolute pixel-wise deviation of the predicted irradiance by the U-Net with the ray-traced irradiance as a measure, the differences are clearly

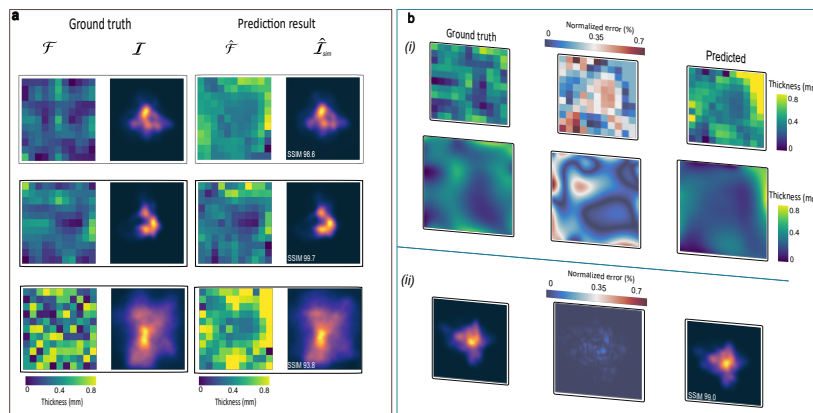


Figure 4: Freeform prediction results for certain validation cases. **(a)** Ground truth ( $\mathcal{F}, \mathcal{I}$ ) against the predicted freeform matrix ( $\hat{\mathcal{F}}$ ) and corresponding MC simulated irradiance ( $\hat{\mathcal{I}}_{sim}$ ) using 1 million rays. **(b)** (i) Pixel-wise error for the normalized predicted freeform surface control points  $|\mathcal{F} - \hat{\mathcal{F}}|$  as well as the interpolated NURBS surfaces. (ii) Pixel-wise error for the simulated irradiances. Notice the significant difference in freeform surface topology (i) while producing an almost identical irradiance distribution (ii).

smaller when comparing to the simulated sample with 1 million rays, even though the model has been trained on the more noisy samples. This convincingly demonstrates that the model is not solely capable of reproducing ray-tracing, but it also denoises the samples that it was trained on.

Given that the model is capable of generating accurate irradiance distributions, it can be used as a rapid alternative for the computationally intensive MC ray-tracing simulations. Following this logic, a synthetic dataset of 3.4 million freeform  $\mathcal{F}$  - irradiance  $\mathcal{I}$  pairs was rapidly generated within minutes. This enables learning on a large synthetic dataset of input irradiance distributions that are a result of the considered freeform topology, enhancing generalization and reducing over-fitting for the more complex, reverse freeform prediction task. The 3.4 million irradiance samples were again separated in a 90-10 train-validation split.

**Freeform prediction on validation data.** Figure 4a shows quantitative and visual results for the freeform prediction model. Inference is done in 11ms for a single sample, and can be even further enhanced with a TensorRT-optimized module. The predicted results are studied for three validation cases, with in each case, a ground truth freeform  $\mathcal{F}$  - irradiance  $\mathcal{I}$  pair is compared with the predicted freeform control points  $\hat{\mathcal{F}}$  by the CNN encoder network and the resulting irradiance distribution with this predicted

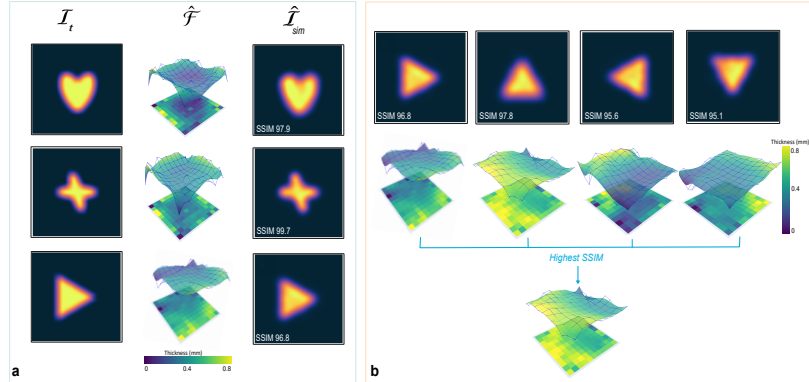


Figure 5: Freeform prediction results for certain custom target irradiances  $\mathcal{I}_t$ . **(a)**  $\mathcal{I}_t$  against the predicted freeform surface topologies  $\hat{\mathcal{F}}$  and the MC ray-traced irradiance  $\hat{\mathcal{I}}_{sim}$ , resulting from  $\hat{\mathcal{F}}$ . **(b)** Rotate test-time augmentation on the triangular target. The results illustrate the existence of various freeform surface topologies that produce almost visually identical irradiance distributions.

freeform ( $\hat{\mathcal{I}}_{sim}$ ). The resulting irradiance distribution has been simulated with MC ray-tracing using an extensive ray-set of 1 million rays, rather than with the U-net model used in the training. This assures a fair assessment of the capabilities of the model to predict an  $\hat{\mathcal{F}}$  that results in a prescribed  $\mathcal{I}$  via ray-tracing. A quantitative assessment of the freeform prediction accuracy is provided by again considering the SSIM between the input  $\mathcal{I}$  and the ray-traced irradiance distribution  $\hat{\mathcal{I}}_{sim}$ . The visual similarity between  $\mathcal{I}$  and  $\hat{\mathcal{I}}_{sim}$  illustrates the performance of the developed framework. However, one also notices the visual discrepancy between  $\mathcal{F}$  and  $\hat{\mathcal{F}}$ . Figure 4b considers this discrepancy more in detail for one specific case, and shows that the pixel-wise deviation for the freeform control points and the interpolated NURBS topologies is much higher than for the irradiance distributions, a feature that is witnessed for most of the validation cases. This observation supports the hypothesis that radically different freeform surface topologies can produce visually identical irradiance distributions. Therefore, training for SSIM on the pseudo-labeled U-net irradiance versus the targeted irradiance is a more logical approach than training for mean average error of the predicted freeform surface compared to the ground truth.

**Freeform prediction on custom targets.** The model performance is also verified in terms of predicting freeform topologies that produce prescribed irradiance distributions, which are neither in the training nor in the validation set. This is the main target of the developed framework. Fig. 5a

shows an overview of the results for three chosen irradiance patterns ( $\mathcal{I}_t$ ). The predicted freeform surface topology ( $\hat{\mathcal{F}}$ ) and corresponding ray-traced irradiance pattern ( $\hat{\mathcal{I}}_{sim}$ ) are given, together with the SSIM of the simulated pattern with respect to the prescribed irradiance. The results clearly indicate that the model is capable of producing fairly complicated freeform surface topologies that closely match the target irradiance distributions. Still, one could wonder if the model produces the best freeform topology prediction in terms of SSIM, since there is no ray-traced ground truth in this case. As a test, a *rotate test-time augmentation* is applied by considering all  $90^\circ$ -rotations of the target pattern. The obtained freeform topologies with the resulting MC-simulated irradiance and corresponding SSIM values are shown in Fig. 5b. These results re-affirm that multiple freeform topologies can result in nearly-identical irradiance patterns and the model finds one of these topologies. In other words, the inverse problem is ill-posed, at least within the limitations of MC ray-tracing. From a practical point-of-view however, such rotational test-time augmentations, or similar alternatives, could prove interesting to generate multiple solutions, out of which the best performing, most smooth or most varying option could be selected, depending on the specific application.

**Training performance.** Finally, the efficiency of the proposed training approach is assessed through a comparative analysis with two alternative methodologies.

- (a) Training in a supervised manner, on L1 loss between  $\mathcal{F}$  and  $\hat{\mathcal{F}}$ , using the full synthetic dataset.
- (b) Training on the SSIM loss with pseudo-labeled irradiances, but using the 25000 MC ray-traced irradiance samples instead of the predicted irradiances by the U-net-SRCNN model.

Fig. 6 considers two target distributions to illustrate the main performance differences: an irradiance distribution from the validation set linked to an actual freeform topology, and a custom prescribed irradiance. For both cases, the regression activation maps (RAM) and resulting ray-traced irradiances  $\hat{\mathcal{I}}_{sim}$  from the predicted freeform topologies are shown for method (a) and (b), compared to the proposed approach. Regression activation maps are included since they provide a detailed representation of how a model localizes discriminative regions affecting the regression outcome [57]. Comparing RAM for the first target pattern, it is visible that method (a) fails to produce confident feature maps at relevant locations. In comparison, model

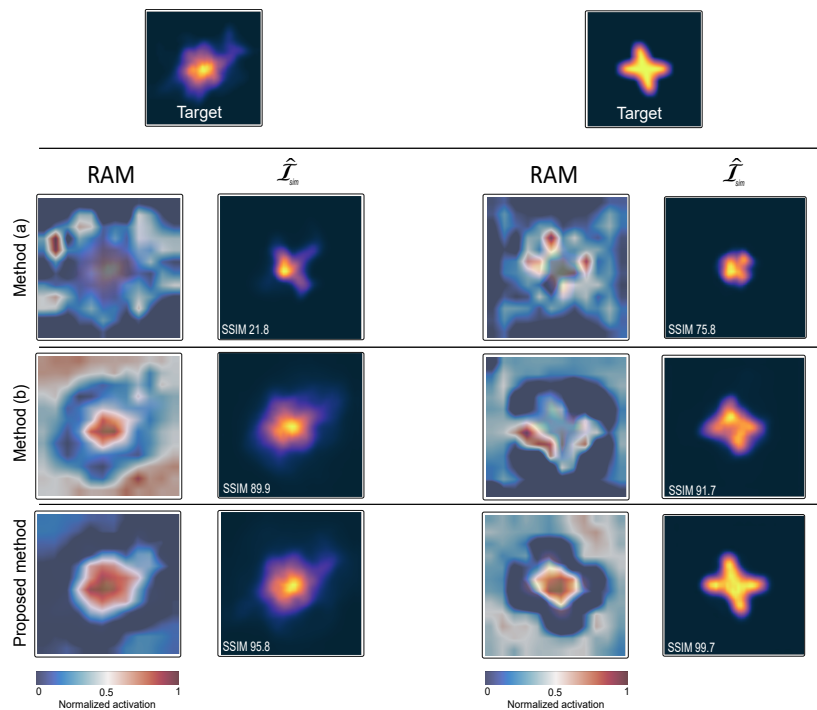


Figure 6: Performance comparison of three different learning approaches. Regression activation maps (RAM, normalized) and the produced irradiance ( $\hat{\mathcal{I}}_{sim}$ ) of the predicted freeform topology  $\hat{\mathcal{I}}$  are shown, both for a target irradiance from the validation set and a custom target irradiance.

(b) manages to locate the core of the supplied irradiance as the most relevant area, but some noise remains. The proposed training method clearly delivers the most accurate localization, with activation maps that overlap with the target distribution. This results in the highest SSIM value for the corresponding ray-traced irradiance. Similar results can be seen for the custom target distribution. In this case, the benefit of relying on synthetic data over the base MC ray-traced data (method b) is visually clear when looking at the obtained irradiance distribution.

## Discussion

This paper presents a semi-supervised learning framework for predicting refractive freeform topologies that produce a certain target irradiance. In contrast to prior work on machine learning for freeform design that predom-

inantly relies on 1D multi-layer perceptron-like networks with contextual information, this study employs 2D convolutional neural networks (CNN) to model the relationship between the obtained irradiance and freeform topology. To train the network, a U-net is used for modeling the Monte-Carlo ray-tracing of light from an extended light source, in order to generate pseudo-labeled irradiance distributions that are compared with the input target irradiances. We demonstrate that this semi-supervised learning approach for freeform topology prediction is superior compared to a supervised learning approach using ground truth freeform topology/irradiance pairs. The resulting framework offers an end-to-end solution for rapid, smooth freeform topology design with extended light sources to produce an arbitrary prescribed target irradiance. The framework is trained within a specific optical setting, using a restricted parameterization for the freeform lens topology. This implies that the model is only capable of predicting freeform components within this parameterization and for the considered illumination setting. Despite these limitations, the proposed framework offers significant opportunities regarding the design and implementation of novel freeform optics.

The fact that freeform topologies can be rapidly generated is especially interesting when considering their implementation on spatial light modulators (SLMs). Modern phase-only SLMs are capable of modulating the optical path length of visible light by multiple wavelengths. This allows to use these SLMs as a kind of programmable freeform optics, by translating a freeform refractive surface into a smooth phase retardation pattern [58, 59]. Despite phase shifts of multiples of  $2\pi$ , wrapping this smooth retardation pattern remains necessary, which causes undesired diffraction effects (i.e. chromatic shift). This effect is more pronounced when targeting non-paraxial illumination [55]. Furthermore, also the fast calculation of the freeform surfaces, required to work in real-time, is very challenging when considering non-paraxial illumination with an extended light source. Both limitations can be addressed with the proposed framework. Indeed, the restricted depth of the predicted freeform topologies allows to eliminate or reduce the required phase jumps when targeting non-paraxial illumination. Also the real-time calculation of freeform topologies that generate fast-changing target irradiance distributions from an extended light source is certainly possible.

The freeform components that are introduced in this paper, with their smooth oscillating surface topology and resulting limited thickness, could also serve as a novel passive beam shaping technology. Current freeform micro-optical components always consist of a periodic array of multiple in-

dividual lenses or mirrors [60, 61], and while the fabrication of such components has evolved significantly over the past years, the inevitable grooves in between the different lens/mirror elements still pose significant manufacturing challenges in order to avoid stray light [62]. The smooth surface topologies that result from the proposed network, avoid such strong surface C2 discontinuities, while still allowing non-paraxial illumination targets. A versatile test-time augmentation strategy can furthermore help to identify the most smooth surface topology to create a certain illumination target.

Finally, the proposed framework and training method could be extended to other, more general freeform illumination design problems. A straightforward extension would be a surface topology parametrization with more control points. This could allow the generation of even more complex irradiance targets, although it should be clear that the extended light source in combination with a single freeform surface also imposes a limitation in this respect. A more interesting expansion from a practical point of view, could be the extension of the framework to various illumination settings and arbitrary extended light sources. This could be realized by introducing additional contextual data to the training of the 2D-CNN network, e.g. the size of/distance to the receiver plane, and/or the position/various characteristics of the extended light source. In a further stage, multiple freeform surfaces could be considered.

While the presented semi-supervised learning strategy proves superior to a supervised learning strategy, for the prediction of shallow freeform surface topologies, it remains to be seen if this would also be the most effective strategy for the design of strictly convex/ concave freeform surfaces. The training of such a framework would certainly require a more specific surface parameterization that enforces concaveness or convexness. Alternatively, contextual data about the freeform shape could be added in the training phase of the 2D-CNN. Whatever the outcome, also in this case, the use of an additional network for modeling the ray-tracing will result in much faster and more effective training.

The discussion above makes clear that the investigation of advanced machine learning techniques for the design of freeform optics has only been started. In this respect, the proposed framework can serve as a convincing demonstration that deep learning allows rapid and standalone freeform optical design.

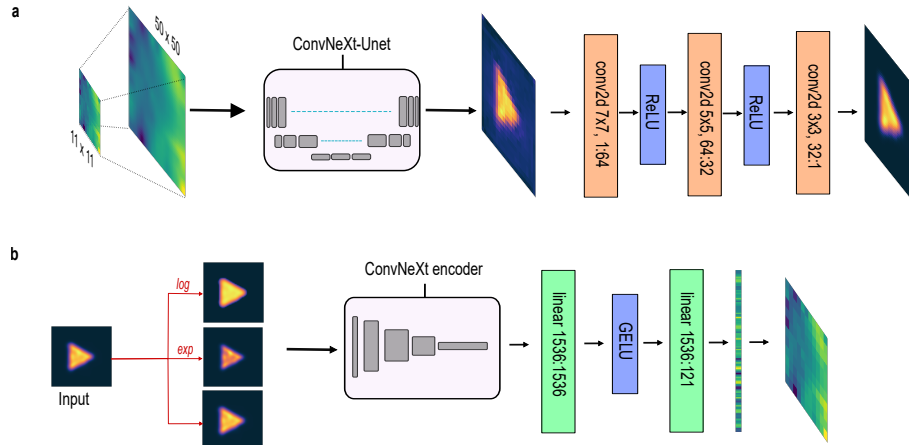


Figure 7: **(a)** U-net-SRCNN model with a more in depth visualization of how the control points are interpolated and how the SRCNN constructs the final irradiance distribution. **(b)** The freeform prediction model, with highlights on the input transformations and the MLP structure that predicts the freeform surface control points.

## Methods

### Data augmentation

Data augmentation is attained by considering the inverse 4-fold rotational symmetry of a freeform surface  $\mathcal{F}$  and the corresponding irradiance distribution  $\mathcal{I}$ . In particular, since a freeform topology is characterized by a square  $11 \times 11$  grid, its rotation results in a reverse rotation of the irradiance distribution via ray-tracing. In short:

$$\text{rot}(90, \mathcal{F}) \rightarrow \text{rot}(-90, \mathcal{I}), \quad (4)$$

where  $\rightarrow$  represents ray-tracing. By considering this symmetry, each freeform surface may be rotated clockwise 3 times, resulting in 3 augmented freeform-illumination pairs for training the U-Net.

### Ray-tracing model (U-Net)

The ray-tracing model receives an  $11 \times 11$  matrix of control points that unambiguously determine the considered freeform surface topology. This matrix is then interpolated to match the CNN kernels (bilinear,  $50 \times 50$ ).

The resulting matrix then passes through a U-net encoder-decoder structure, with the encoder being the state-of-the-art, fully convolutional ConvNeXt [63] (Fig. 7a). Drop path rate is used to prevent over-fitting [64]. The U-net output is a  $25 \times 25$  pixel irradiance, which is up-scaled (bilinear) to  $50 \times 50$  pixels. Consequently the up-scaled images are passed through a trainable SRCNN architecture [51] with non-linear (ReLU) transformations and kernel sizes of 7, 5 and 3, respectively.

### Loss function

The U-net-SRCNN model is trained based on the structural similarity index measure (SSIM) loss. The Structural Similarity Index (SSIM) measure is defined as [52]:

$$\text{SSIM}(x, y) = \frac{(2\mu_x\mu_y + C_1)(2\sigma_{xy} + C_2)}{(\mu_x^2 + \mu_y^2 + C_1)(\sigma_x^2 + \sigma_y^2 + C_2)}$$

where  $x$  and  $y$  represent the horizontal and vertical directions within an image, and  $\mu$  and  $\sigma$  the variance. Furthermore,  $\sigma_{xy}$  is the covariance of both directions, and  $C_1$  and  $C_2$  are constants that stabilize the nominator and denominator in the calculation. SSIM is used since it considers luminance and contrast perception, contrary to the commonly used mean average error (MAE). SSIM outputs a fraction between 0 and 1, implying that the loss to be minimized between an irradiance  $\mathcal{I}$  and its prediction  $\hat{\mathcal{I}}$  is:

$$1 - \text{SSIM}(\mathcal{I}, \hat{\mathcal{I}}). \quad (5)$$

### Freeform prediction model

The main component of the freeform prediction architecture is a CNN encoder, which is ConvNeXt [63]. The model takes a 3-channel image as input, consisting of:

$$\{\mathcal{I}, \log(\mathcal{I}), \exp(\mathcal{I})\}. \quad (6)$$

Using the logarithmic and exponential transforms of  $\mathcal{I}$  allows the model to explore the global and local properties more easily (Fig. 7b). The model head contains a 2D max-pooling layer, which is a  $2 \times 2$  filter that runs over all the extracted feature maps, maintaining the maximal value as the output. This significantly reduces over-fitting. The max-pooling output is passed through a non-linear mapping MLP that outputs 121 variables, with GELU activation. The output is then reshaped into a  $11 \times 11$  grid  $\hat{\mathcal{F}}$  of freeform topology control points.

The model is trained in a semi-supervised manner: for each predicted set of control points, the corresponding irradiance distribution is computed and compared with the input. The irradiance distribution is calculated as a pseudo-labeled image via the pre-trained U-net-SRCNN model. If this U-net-SRCNN model is represented by  $\mathbf{R}$ , the loss function on which the model is trained is:

$$1 - \text{SSIM}(\mathcal{I}, \mathbf{R}(\hat{\mathcal{F}})), \quad (7)$$

with  $\mathcal{I}$  the input irradiance into the network.

### Training setup

All models in the proposed method use ImageNet-21k pre-trained weights [65], although the contribution of these is likely limited. Training is done using exponential learning rate decay with linear warm-up. A full overview of the training, as well as the used encoder variant, is shown in Table 1. For the freeform prediction models, the training procedure is given for each of the methods discussed in the training performance section.

	U-net-SRCNN	Freeform prediction		
		Method (a)	Method (b)	Proposed method
Optimizer	AdamW[66]	AdamW[66]	AdamW[66]	AdamW[66]
Base learning rate	1e-4	6e-4	2e-4	6e-4
Weight decay	0.05	0.05	0.05	0.05
Warmup epochs	3, linear	5, linear	1, linear	5, linear
Learning rate scheduler	cosine decay	cosine decay	cosine decay	cosine decay
Training epochs	50	20	25	20
Batch size	512	196	512	196
Augmentations	randomflip[Eq. 4]	randomflip[Eq. 4]	randomflip[Eq. 4]	randomflip[Eq. 4]
Encoder variant	<i>ConvNeXt-base</i> [63]	<i>ConvNeXt-large</i> [63]	<i>ConvNeXt-tiny</i> [63]	<i>ConvNeXt-large</i> [63]
Drop path rate	0.05	0.1	0	0.1
Full data size	25000	3.4 million	25000	3.4 million

Table 1: Full training set-up for all the considered models.

## References

- [1] Caulfield, H. J. & Dolev, S. Why future supercomputing requires optics. *Nature Photonics* **4**, 261–263 (2010).
- [2] Capasso, F. The future and promise of flat optics: a personal perspective. *Nanophotonics* **7**, 953–957 (2018).
- [3] Nikolov, D. K. *et al.* Metaform optics: bridging nanophotonics and freeform optics. *Science Advances* **7**, eabe5112 (2021).

- [4] Duerr, F. & Thienpont, H. Freeform imaging systems: Fermat’s principle unlocks “first time right” design. *Light: Science & Applications* **10**, 95 (2021).
- [5] Volatier, J.-B. & Druart, G. Differential method for freeform optics applied to two-mirror off-axis telescope design. *Optics letters* **44**, 1174–1177 (2019).
- [6] Reimers, J., Bauer, A., Thompson, K. P. & Rolland, J. P. Freeform spectrometer enabling increased compactness. *Light: Science & Applications* **6**, e17026–e17026 (2017).
- [7] Zhang, B., Jin, G. & Zhu, J. Towards automatic freeform optics design: coarse and fine search of the three-mirror solution space. *Light: Science & Applications* **10**, 65 (2021).
- [8] Jahn, W., Ferrari, M. & Hugot, E. Innovative focal plane design for large space telescope using freeform mirrors. *Optica* **4**, 1188–1195 (2017).
- [9] Li, J. *et al.* Two-photon polymerisation 3d printed freeform micro-optics for optical coherence tomography fibre probes. *Scientific reports* **8**, 14789 (2018).
- [10] Yang, T., Jin, G.-F. & Zhu, J. Automated design of freeform imaging systems. *Light: Science & Applications* **6**, e17081–e17081 (2017).
- [11] Yang, T., Zhu, J., Wu, X. & Jin, G. Direct design of freeform surfaces and freeform imaging systems with a point-by-point three-dimensional construction-iteration method. *Optics express* **23**, 10233–10246 (2015).
- [12] Wu, R. *et al.* Precise light control in highly tilted geometry by freeform illumination optics. *Optics Letters* **44**, 2887–2890 (2019).
- [13] Wei, S., Zhu, Z., Fan, Z. & Ma, D. Least-squares ray mapping method for freeform illumination optics design. *Optics express* **28**, 3811–3822 (2020).
- [14] Wu, R. *et al.* Design of freeform illumination optics. *Laser & Photonics Reviews* **12**, 1700310 (2018).
- [15] Ibrahim, K. A., Mahecic, D. & Manley, S. Characterization of flat-fielding systems for quantitative microscopy. *Optics Express* **28**, 22036–22048 (2020).

- [16] Desnijder, K., Hanselaer, P. & Meuret, Y. Ray mapping method for off-axis and non-paraxial freeform illumination lens design. *Optics letters* **44**, 771–774 (2019).
- [17] Wu, R. *et al.* Freeform illumination design: a nonlinear boundary problem for the elliptic monge–ampère equation. *Optics letters* **38**, 229–231 (2013).
- [18] Madrid-Sánchez, A., Duerr, F., Nie, Y., Thienpont, H. & Ottevaere, H. Freeform optics design method for illumination and laser beam shaping enabled by least squares and surface optimization. *Optik* **269**, 169941 (2022).
- [19] Prins, C., ten Thije Boonkkamp, J., Van Roosmalen, J., Jzerman, W. & Tukker, T. W. A monge–ampère-solver for free-form reflector design. *SIAM Journal on Scientific Computing* **36**, B640–B660 (2014).
- [20] Bösel, C. & Gross, H. Compact freeform illumination system design for pattern generation with extended light sources. *Applied optics* **58**, 2713–2724 (2019).
- [21] Birch, D. A. & Brand, M. Design of freeforms to uniformly illuminate polygonal targets from extended sources via edge ray mapping. *Applied Optics* **59**, 6490–6496 (2020).
- [22] Sorgato, S., Chaves, J., Thienpont, H. & Duerr, F. Design of illumination optics with extended sources based on wavefront tailoring. *Optica* **6**, 966–971 (2019).
- [23] Dross, O. *et al.* Review of sms design methods and real world applications. In *Nonimaging optics and efficient illumination systems*, vol. 5529, 35–47 (SPIE, 2004).
- [24] Byzov, E. V., Kravchenko, S. V., Moiseev, M. A., Bezus, E. A. & Doskolovich, L. L. Optimization method for designing double-surface refractive optical elements for an extended light source. *Optics Express* **28**, 24431–24443 (2020).
- [25] Wei, S., Zhu, Z., Li, W. & Ma, D. Compact freeform illumination optics design by deblurring the response of extended sources. *Optics Letters* **46**, 2770–2773 (2021).

- [26] Liu, Z., Liu, P. & Yu, F. Parametric optimization method for the design of high-efficiency free-form illumination system with a led source. *Chinese Optics Letters* **10**, 112201–112201 (2012).
- [27] Fournier, F. & Rolland, J. Optimization of freeform lightpipes for light-emitting-diode projectors. *Applied optics* **47**, 957–966 (2008).
- [28] Mao, X., Li, H., Han, Y. & Luo, Y. Two-step design method for highly compact three-dimensional freeform optical system for led surface light source. *Optics Express* **22**, A1491–A1506 (2014).
- [29] Situ, W., Han, Y., Li, H. & Luo, Y. Combined feedback method for designing a free-form optical system with complicated illumination patterns for an extended led source. *Optics express* **19**, A1022–A1030 (2011).
- [30] Wang, C., Chen, N. & Heidrich, W. do: A differentiable engine for deep lens design of computational imaging systems. *IEEE Transactions on Computational Imaging* **8**, 905–916 (2022).
- [31] Nie, Y., Zhang, J., Su, R. & Ottevaere, H. Freeform optical system design with differentiable three-dimensional ray tracing and unsupervised learning. *Optics Express* **31**, 7450–7465 (2023).
- [32] Wang, H. *et al.* B-spline freeform surface tailoring for prescribed irradiance based on differentiable ray-tracing. *arXiv preprint arXiv:2303.17108* (2023).
- [33] de Koning, B., Heemels, A., Adam, A. & Möller, M. Gradient descent-based freeform optics design using algorithmic differentiable non-sequential ray tracing. *arXiv preprint arXiv:2302.12031* (2023).
- [34] Wang, H. *et al.* Extended ray-mapping method based on differentiable ray-tracing for non-paraxial and off-axis freeform illumination lens design. *Optics Express* **31**, 30066–30078 (2023).
- [35] Shen, Y. *et al.* Deep learning with coherent nanophotonic circuits. *Nature photonics* **11**, 441–446 (2017).
- [36] Wiecha, P. R., Arbouet, A., Girard, C. & Muskens, O. L. Deep learning in nano-photonics: inverse design and beyond. *Photonics Research* **9**, B182–B200 (2021).

- [37] Xu, Y., Zhang, X., Fu, Y. & Liu, Y. Interfacing photonics with artificial intelligence: an innovative design strategy for photonic structures and devices based on artificial neural networks. *Photonics Research* **9**, B135–B152 (2021).
- [38] Gao, L., Chai, Y., Zibar, D. & Yu, Z. Deep learning in photonics: Introduction. *Photonics Research* **9**, DLP1–DLP3 (2021).
- [39] Eybposh, M. H., Caira, N. W., Atisa, M., Chakravarthula, P. & Pégard, N. C. Deepcgh: 3d computer-generated holography using deep learning. *Optics Express* **28**, 26636–26650 (2020).
- [40] Shimobaba, T. *et al.* Deep-learning computational holography: A review. *Frontiers in Photonics* **3**, 8 (2022).
- [41] Mao, B. *et al.* Freeformnet: fast and automatic generation of multiple-solution freeform imaging systems enabled by deep learning. *Photonics Research* **11**, 1408–1422 (2023).
- [42] Chen, W., Yang, T., Cheng, D. & Wang, Y. Generating starting points for designing freeform imaging optical systems based on deep learning. *Optics Express* **29**, 27845–27870 (2021).
- [43] Yang, T., Cheng, D. & Wang, Y. Direct generation of starting points for freeform off-axis three-mirror imaging system design using neural network based deep-learning. *Optics express* **27**, 17228–17238 (2019).
- [44] Gannon, C. & Liang, R. Using machine learning to create high-efficiency freeform illumination design tools. *arXiv preprint arXiv:1903.11166* (2018).
- [45] Desnijder, K. *et al.* Design of a freeform, luminance spreading illumination lens with a continuous surface. In *Illumination Optics V*, vol. 10693, 89–99 (SPIE, 2018).
- [46] Desnijder, K., Ryckaert, W., Hanselaer, P. & Meuret, Y. Luminance spreading freeform lens arrays with accurate intensity control. *Optics Express* **27**, 32994–33004 (2019).
- [47] Zhu, W.-L., Duan, F., Zhang, X., Zhu, Z. & Ju, B.-F. A new diamond machining approach for extendable fabrication of micro-freeform lens array. *International Journal of Machine Tools and Manufacture* **124**, 134–148 (2018).

- [48] Desnijder, K., Hanselaer, P. & Meuret, Y. Freeform fresnel lenses with a low number of discontinuities for tailored illumination applications. *Optics express* **28**, 24489–24500 (2020).
- [49] Ronneberger, O., Fischer, P. & Brox, T. U-net: Convolutional networks for biomedical image segmentation. In *Medical Image Computing and Computer-Assisted Intervention–MICCAI 2015: 18th International Conference, Munich, Germany, October 5-9, 2015, Proceedings, Part III 18*, 234–241 (Springer, 2015).
- [50] Yanny, K., Monakhova, K., Shuai, R. W. & Waller, L. Deep learning for fast spatially varying deconvolution. *Optica* **9**, 96–99 (2022).
- [51] Dong, C., Loy, C. C., He, K. & Tang, X. Image super-resolution using deep convolutional networks. *IEEE transactions on pattern analysis and machine intelligence* **38**, 295–307 (2015).
- [52] Wang, Z., Bovik, A. C., Sheikh, H. R. & Simoncelli, E. P. Image quality assessment: from error visibility to structural similarity. *IEEE transactions on image processing* **13**, 600–612 (2004).
- [53] Lee, C., Song, G., Kim, H., Ye, J. C. & Jang, M. Deep learning based on parameterized physical forward model for adaptive holographic imaging with unpaired data. *Nature Machine Intelligence* 1–11 (2023).
- [54] Lee, D.-H. *et al.* Pseudo-label: The simple and efficient semi-supervised learning method for deep neural networks. In *Workshop on challenges in representation learning, ICML*, vol. 3, 896 (Atlanta, 2013).
- [55] Rondelez, N., Desnijder, K., Ryckaert, W. & Meuret, Y. Programmable freeform optics with extended white light sources: possibilities and limitations. *Optics Express* **31**, 1303–1317 (2023).
- [56] Lighttools 8.7.0, synopsys optical solutions, mountain view, california 2019.
- [57] Wang, Z. & Yang, J. Diabetic retinopathy detection via deep convolutional networks for discriminative localization and visual explanation. *arXiv preprint arXiv:1703.10757* (2017).
- [58] Damberg, G. & Heidrich, W. Efficient freeform lens optimization for computational caustic displays. *Optics express* **23**, 10224–10232 (2015).

- [59] Bawart, M., Bernet, S. & Ritsch-Marte, M. Programmable freeform optical elements. *Optics Express* **25**, 4898–4906 (2017).
- [60] Aderneuer, T. *et al.* Surface topology and functionality of freeform microlens arrays. *Optics Express* **29**, 5033–5042 (2021).
- [61] Bec, J., Li, C. & Marcu, L. Broadband, freeform focusing micro-optics for a side-viewing imaging catheter. *Optics letters* **44**, 4961–4964 (2019).
- [62] Kumar, S., Tong, Z. & Jiang, X. Advances in the design and manufacturing of novel freeform optics. *International Journal of Extreme Manufacturing* **4**, 032004 (2022).
- [63] Liu, Z. *et al.* A convnet for the 2020s. In *Proceedings of the IEEE/CVF Conference on Computer Vision and Pattern Recognition*, 11976–11986 (2022).
- [64] Larsson, G., Maire, M. & Shakhnarovich, G. Fractalnet: Ultra-deep neural networks without residuals. *arXiv preprint arXiv:1605.07648* (2016).
- [65] Ridnik, T., Ben-Baruch, E., Noy, A. & Zelnik-Manor, L. Imagenet-21k pretraining for the masses. *arXiv preprint arXiv:2104.10972* (2021).
- [66] Loshchilov, I. & Hutter, F. Decoupled weight decay regularization. *arXiv preprint arXiv:1711.05101* (2017).